Available online at www.sciencedirect.com

SciVerse ScienceDirect

Journal of the European Ceramic Society 32 (2012) 807–814

www.elsevier.com/locate/jeurceramsoc

Laser machining of Al_2O_3–ZrO_2 (3%Y_2O_3) eutectic composite

D. Sola [a,*], J.I. Peña [b]

[a] Centro de Física de Materiales, Universidad del País Vasco-CSIC, Departamento de Física Aplicada I, Alda. de Urquijo s/n, 48,013 Bilbao, Spain
[b] Instituto de Ciencia de Materiales de Aragón, Universidad de Zaragoza-CSIC, Departamento de Ciencia y Tecnología de Materiales y Fluidos, C/María de Luna 3, 50,018 Zaragoza, Spain

Received 20 September 2011; accepted 1 November 2011
Available online 26 November 2011

Abstract

In this work we present the study of the interaction between NIR pulsed laser and Al_2O_3–ZrO_2 (3%Y_2O_3) eutectic composite. The effect produced by modifying the reference position as well as the working conditions and laser beam features has been studied when the samples are processed by means of pulse bursts.

The samples were obtained by the laser floating zone technique using a CO_2 laser system. The laser machining was carried out with a Q-switched Nd:YAG laser at its fundamental wavelength of 1064 nm with pulse-widths in the nanosecond range.

Geometric dimensions, i.e. ablated depth, machined width and removed volume as well as ablation yield of the resulting holes have been studied. We have described and discussed the morphology, composition and microstructure of the processed samples.

Keywords: Laser machining; Al_2O_3; ZrO_2; Wear resistance; Functional applications

1. Introduction

Laser processing is of great interest in the field of optics, electronics, microelectronics, aerospace and medicine. This technique is cost-effective compared to traditional methods and it may be applied to a wide range of substrates, such as metals, ceramics and semiconductors.[1] In the field of materials processing by laser, several methods, such as laser machining, micromachining, marking, drilling and pulsed laser deposition, have been developed along the last two decades.[2,3]

The appearance of techniques for generating short and ultrashort laser pulses, ranging from tens of nanoseconds to a few femtoseconds without variation of other parameters such as pulse energy or the working frequency, have allowed the availability of more powerful systems, with power densities that can reach TW/cm^2. These laser systems, with better features and lower prices, offer a high-speed/high-quality tool for laser machining, which is of great interest in both basic and applied research for scientific and technological purposes.[3,4]

However, the foundations of the mechanisms involved in laser ablation are far from being well established. It is known that laser ablation depends on laser wavelength, optical features of laser beam, pulse-width regime and optical-thermal-mechanical properties of the substrate. Some theoretical descriptions have been developed by many authors to generalize the stages of the ablation process.[4–19]

Directionally solidified eutectic ceramics are commonly employed for functional and structural components because of their features, amongst which is worthy of mentioning their lightness, hardness, wear resistance and chemical stability at high temperature.[20–22] In particular, the eutectic composites based in Al_2O_3 are of great interest because of the properties derived from the distribution of the phases after solidification which can provide them with high flexural strength, toughness and creep resistance at high temperature and structural stability up to temperatures close to melting point, making them good candidates for applications such as gas turbines or systems for energy generation.[23,24]

In this work the interaction between NIR pulsed laser in the nanosecond range and the Al_2O_3–ZrO_2 (3%Y_2O_3) eutectic composite, directionally solidified, has been investigated to modified the surface in order to improve the wear behavior. The role the topography of the surface plays is of paramount

* Corresponding author. Tel.: +34 946014051; fax: +34 946014178.
E-mail addresses: dsola@unizar.es, daniel_sola@ehu.es (D. Sola).

0955-2219/$ – see front matter © 2011 Elsevier Ltd. All rights reserved.
doi:10.1016/j.jeurceramsoc.2011.11.007

Table 1
Laser output parameters.

	Working frequency				
	1	2	5	10	40
Pulse energy (mJ)[a]	2.7	2.45	1.6	0.9	0.5
Pulse length FWHM (ns)[a]	8	10	12	20	40
Peak power (kW)[a]	300	260	120	45	2
Pulse irradiance (GW/cm^2)	226	196	90	34	1.5
Optical absorption $\alpha\|_{1064\,nm}$ (cm^{-1})	2.4	2.4	2.4	2.4	2.4
Absorption length $L_\alpha\|_{1064\,nm}$ (cm)	0.42	0.42	0.42	0.42	0.42
Thermal diffusion length L_{th} (μm)	0.21	0.23	0.26	0.33	0.47

[a] Data provided by the laser manufacturer.

importance in aspects of great significance such as friction or wear resistance. The tribological behavior of a system can be improved by machining the surface in order to avoid a flat morphology.[25] The geometry of the machined zones, in cavity or groove shape, and their distribution on the surface are some of the key factors to take into account in the tribological behavior.[26]

The geometrical dimensions and the ablation yield have been investigated since they depend on the reference position, on the laser working conditions as well as in the method of machining.[27]

2. Experimental

2.1. Sample fabrication

The precursor rods were obtained from commercial powders of Al_2O_3 (99.99%, Aldrich), ZrO_2 (3%Y_2O_3) (99.99%, Tosho TZ3YS) and Mn_2O_3 (99.99% Aldrich). The powders were ground in a planetary mill with acetone in an alumina container. They were fired in air for 1 h, hand milled in an agate mortar to eliminate agglomerates and mixed in the eutectic composition: 62% Al_2O_3, 36.9% ZrO_2 and 1.1% of Y_2O_3, expressed in mol%. The resulting powders were isostatic pressed at 200 MPa for 2 min obtaining ceramic rods which were sintered at 1500 °C for 12 h.

The samples that will be tested for wear resistance will be produced by the laser surface melting technique using a focussed diode laser system that emits in 940 nm. To favour the absorption of the laser irradiation, a 0.9% of Mn_2O_3 is incorporated to the eutectic composite. The influence the addition of this oxide to the ceramic composite produces has been investigated by machining samples with and without Mn_2O_3.

The laser floating zone system include a CO_2 semisealed laser of 600 W (Electronic Engineering Blade 600) emitting in 10.6 μm and an in-house built growth chamber with gold coated metal mirrors for the beam focussing and two vertical axis for the cylinder displacement. Both axes have independent rotation and translation movement. A more detailed description of this technique can be consulted elsewhere.[20–24,28–30]

Finally, before the laser machining process, the eutectic fibers were flattened using a rotating sander machine.

2.2. Laser processing

A commercial diode-pumped Nd:YAG laser has been used in this work (Rofin-Sinar E-Line 20). The laser system operates at its fundamental wavelength of 1064 nm with a maximum mean power of 11 watts, in a Gaussian beam mode TEM_{00} with a beam quality factor $M^2 < 1.3$. The opto-acoustical Q-Switch commutator controls the cavity output in continuous and pulsed mode, generating pulses as short as 8 ns with a frequency range of 1–40 kHz.

The beam is deflected by a programmable galvanometer scanner controlled by CAD software, making a bidirectional movement in such a way that any predefined pattern and processing procedure can be performed. The system is equipped with a beam expansor 5× before the galvanometric mirrors and a convex lens with focal length f of 100 mm. Thus, using the equations[1]:

$$D_{bw} = \frac{4FM^2\lambda}{\pi D_0} \quad (1)$$

$$R = \left(\frac{\pi D_{bw}^2}{4M^2\lambda}\right) \quad (2)$$

where D_0 is the diameter of the laser beam before the optical lens, the diameter at the focal point D_{bw} and the Rayleigh range R for this system are, approximately, 13 μm and 96 μm, respectively.

The laser processing was carried out by means of pulse bursts, irradiating with a series of between 5 and 150 laser pulses according to the laser output parameters given in Table 1 and modifying the reference distance.

2.3. Characterization techniques

The microstructure and composition has been determined by means of scanning electron microscopy (SEM) using a JEOL JSM6400 with EDX analysis. Superficial topography, profile and removed volume measurements have been carried out with an optical confocal microscope Nikon Sensofar Plμ2300. Absorbance spectrum was measured using a double beam spectrophotometer UV–Vis–IR Cary 500 Varian.

Table 2
Output diameter D mean values and standard deviation for 1 kHz with and without Mn_2O_3, 2 and 5 kHz.

f (kHz)	D (μm)	σD (μm)
1.00	95.10	6.19
2.00	108.76	7.57
5.00	111.82	7.52
1 + Mn	91.50	7.75

3. Results and discussion

3.1. Laser processing

The geometrical dimensions obtained, i.e. depth Z_p, diameter D_p and removed volume V_p, depend on the optical properties of the laser beam, configuration of the laser system, working parameters and mechanical, optical and thermal properties of the substrate to be processed. Furthermore, two critical lengths that play a key role in the amount of energy absorbed[2,3,31,32] and have to be taken into account are the optical absorption length L_α, defined as the inverse of the optical absorption coefficient α, and the thermal diffusion length L_{th} given by

$$L_{th} = 2\sqrt{D\ \Delta t} \quad (3)$$

where D is the thermal diffusivity and Δt is the pulse length.

In the first instance, in order to favour the machining process the sample was placed slightly out of the focal plane[27] and was processed with bursts between 5 and 150 pulses and frequencies between 1 and 5 kHz.

In Fig. 1 the geometrical dimensions obtained are shown. In all the cases, the addition of Mn_2O_3 was of significance only for low pulse numbers under 50. In the same way, the dispersion observed in the results was greater for low pulse series, in such a way that a homogeneous response of the material required processing the material with at least 25 pulses.

Regarding the mean output diameter, the value obtained remained almost constant with the incoming pulse number NP. However, the variation was very significant with frequency, where the greatest values were obtained for the highest frequencies. In Table 2, where the mean values of the machined diameters are shown, differences of up to a 17% can be appreciated.

On the other hand, the ablated depth and the removed volume increased linearly with the pulse number. There were no significant changes in the ablated depth with frequency variation but the removed volume behaved like the diameter, with the highest amount of material removed for the highest frequencies.

These results showed a loss in the efficiency of the process with the pulse number, as Fig. 2 shows, where the mean geometrical dimensions per pulse in function of the pulse are depicted. This behavior can be explained by the thermal mechanisms activated by the laser beam during the laser ablation process and the variation in the distance to the surface to be machined. On one hand, the ablation process essentially consists in the absorption

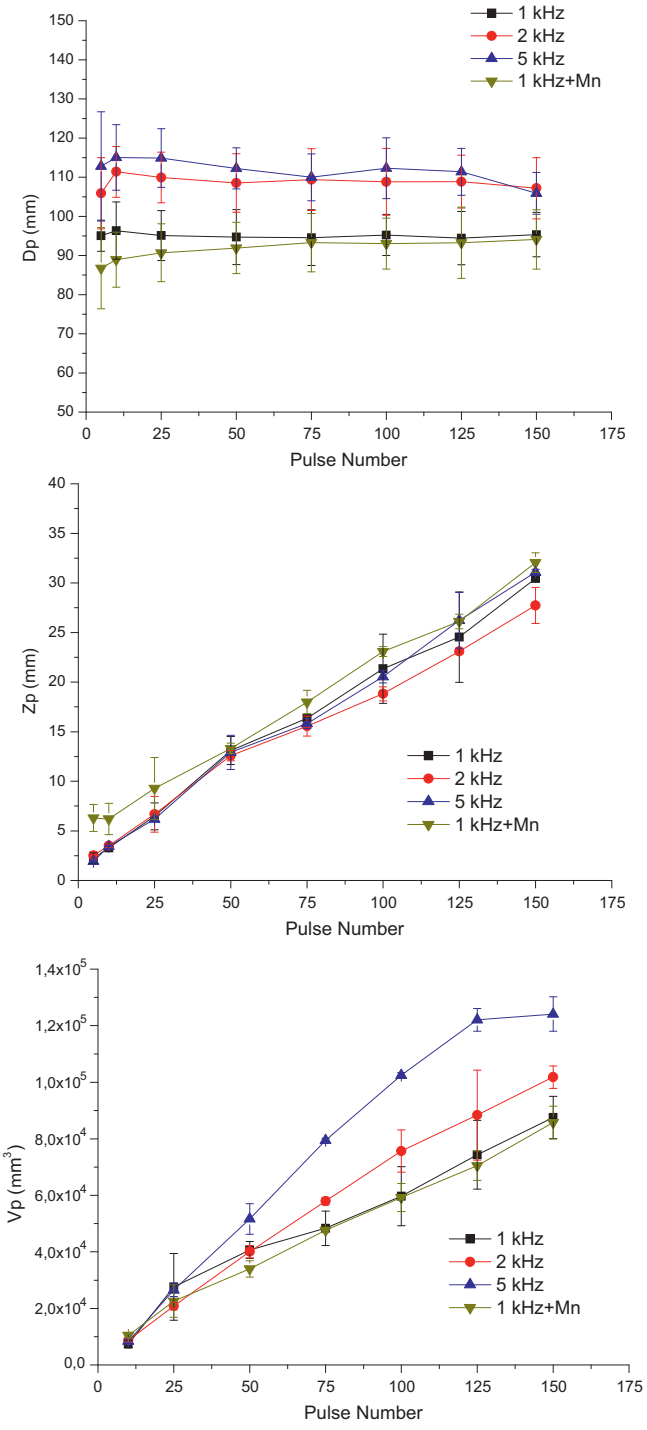

Fig. 1. Geometric parameters in function of pulse number, for 1 kHz with and without Mn_2O_3, 2 and 5 kHz.

of the laser energy and subsequent evaporation and ejection of the material. Taking into account the working conditions and the laser beam features, in this case the ablation process is a photothermal-mechanical one. Thus, a thin layer of material in liquid-phase is formed in the interaction zone,[2] Fig. 3. The recoil pressure produced in the process squeezes the liquid out from the interaction zone and the material is removed from the surface via evaporation and liquid-phase expulsion. The thickness

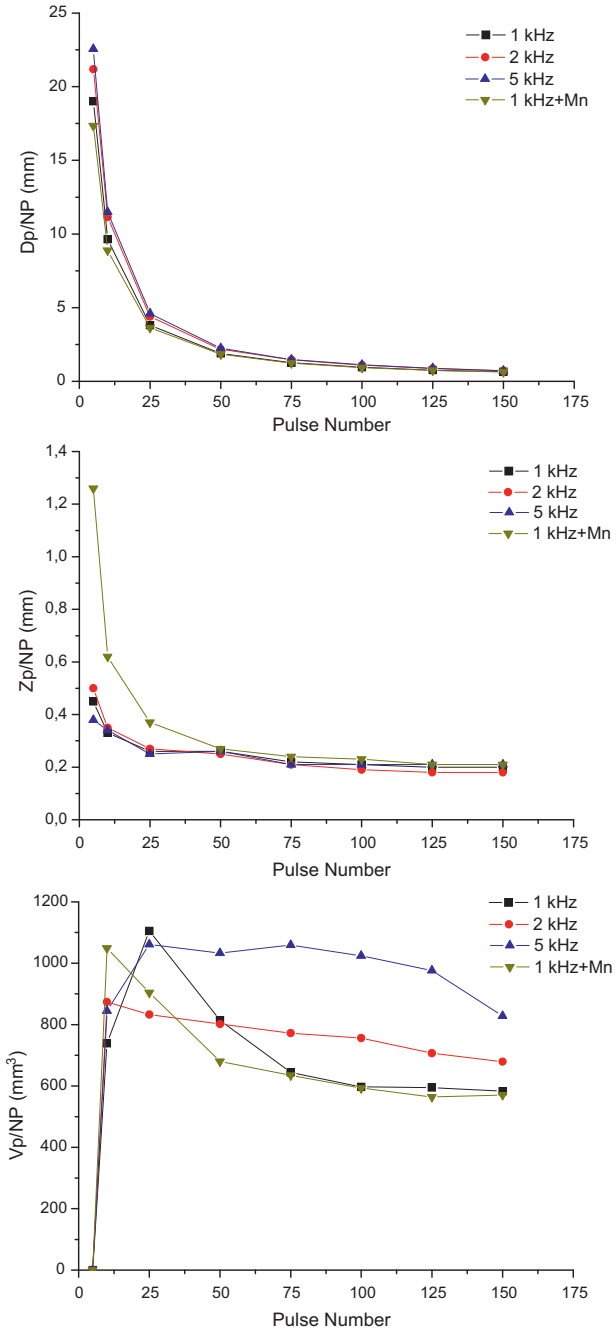

Fig. 2. Mean geometric parameters in function of pulse number, for 1 kHz with and without Mn_2O_3, 2 and 5 kHz.

of liquid phase, h_l, and recoil pressure, P_{rec}, can be expressed as[2]

$$h_l \propto (D)^{1/2}\left(\frac{\Delta H_V}{I_a}\right)^{1/4} \quad (4)$$

$$P_{rec} \approx 10^{-5}\, I_a \quad (5)$$

where D is the thermal diffusivity, ΔH_v the enthalpy of vaporization, and I_a the absorbed laser intensity.

Since the variations of thermal diffusivity and enthalpy of vaporization with temperature are negligible,[33,34] the thickness

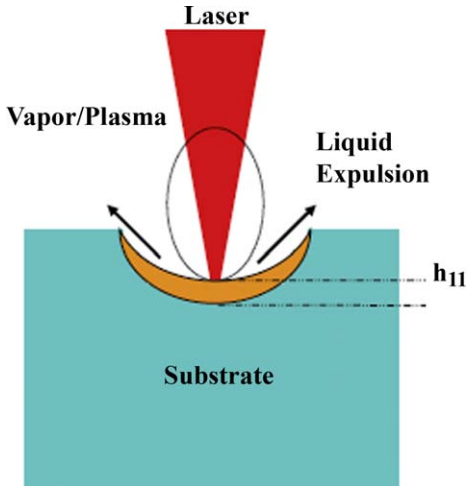

Fig. 3. Scheme of ablation process where the layer of molten material with thickness h_l is shown.

of the molten layer and the recoil pressure depend mainly on the absorbed irradiance.

Furthermore, as the pulse number increases the temperature in the interaction zone is risen,[6,7] resulting in an increase in the thermal agitation of the ions of the lattice. This fact, together with the particles ejected during the process which shield the incoming irradiation, produce a diminution in the effective irradiance and hence, in the recoil pressure produced. This results in an increase of the thickness of the layer in liquid-phase present in the interaction zone in such a way that the ablation process is less efficient.

On the other hand, as the material is removed from the interaction zone the distance to the surface to be machined increases resulting in a diminution in the laser irradiance and therefore, in the efficiency of the process.

It can also be observed that, for the same working conditions, ablated depths of up to three times higher for low pulse number series can be obtained with the addition of Mn_2O_3.

Once the geometrical dimensions were studied, in order to compare the ablation yield of the process, the amount of material removed per unit of delivered energy was calculated, Fig. 4. As can be observed, the lower pulse number the greater dispersion was produced. Furthermore, a slight decrease with the pulse number was observed. More significant is the fact that the yield increased with the working frequency, obtaining the highest value for 5 kHz. Regarding the presence of Mn_2O_3, only when the pulse number was under 50 were the variations produced remarkable.

In the second place, the sample with and without Mn_2O_3 was processed in the surroundings of the focal plane for a whole range of 2.5 mm with bursts of 50 pulses and 1 kHz, Fig. 5. Since the focal point is the place where the beam waist is minimal and the irradiance and the fluence reached are maxima, the diameter and depth obtained were also minimal and maximal at this point. Regarding the volume removed, the value of the diameter predominated over the depth, and thus it was also minimal at the focal point, increasing as the sample was moved away. Further-

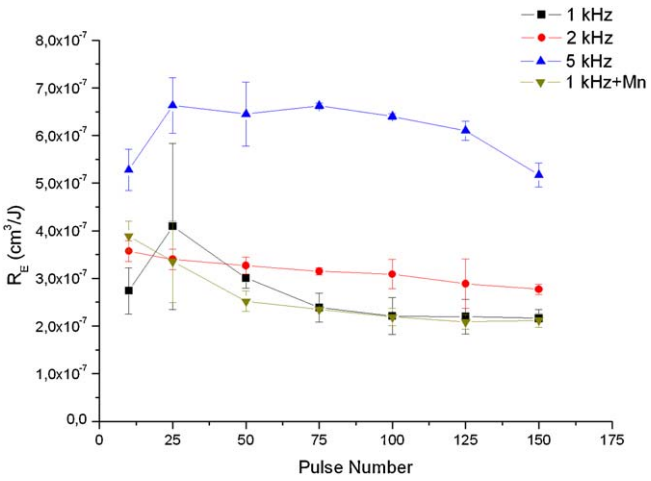

Fig. 4. Ablation yield in function of pulse number, for 1 kHz with and without Mn_2O_3, 2 and 5 kHz.

more, the effect of Mn_2O_3 did not produce significant variations in any of the parameters. As in the study with the pulse number, once the geometrical dimensions were studied, the ablation yield was calculated, Fig. 6. In this case, the ablation yield increased as the sample was moved away from the focal point, reaching differences up to an order of magnitude. In contrast, the addition of Mn_2O_3 was not significant.

Finally, the variation of the geometrical dimensions and ablation yield were studied in function of the working frequency. In this case, the sample was placed at the focal plane and processed with bursts of 50 pulses and frequencies of 1, 2, 5, 10, 20 and 40 kHz. In Fig. 7, a disparity in the behavior of ablated depth with respect to the machined diameter and removed volume was produced. The first one reached its maximum for 10 kHz whilst the latter did it in 5 kHz. Regarding the ablation yield, Fig. 8, the maximum value was reached in 10 kHz, decreasing for higher frequencies.

In this way, the laser interaction process with the eutectic composite depends on factors such as the substrate temperature, the plasma shield, the pulse number, the sample position with respect to the focal plane and the working frequency. Hence, there are no unique optimal machining conditions but they do depend on the purpose of the processing. The working conditions to assign will depend on if the target is to obtain a high ablation yield, to minimize the radiation affected zones, to obtain minimum diameter or maximum ablated depth.

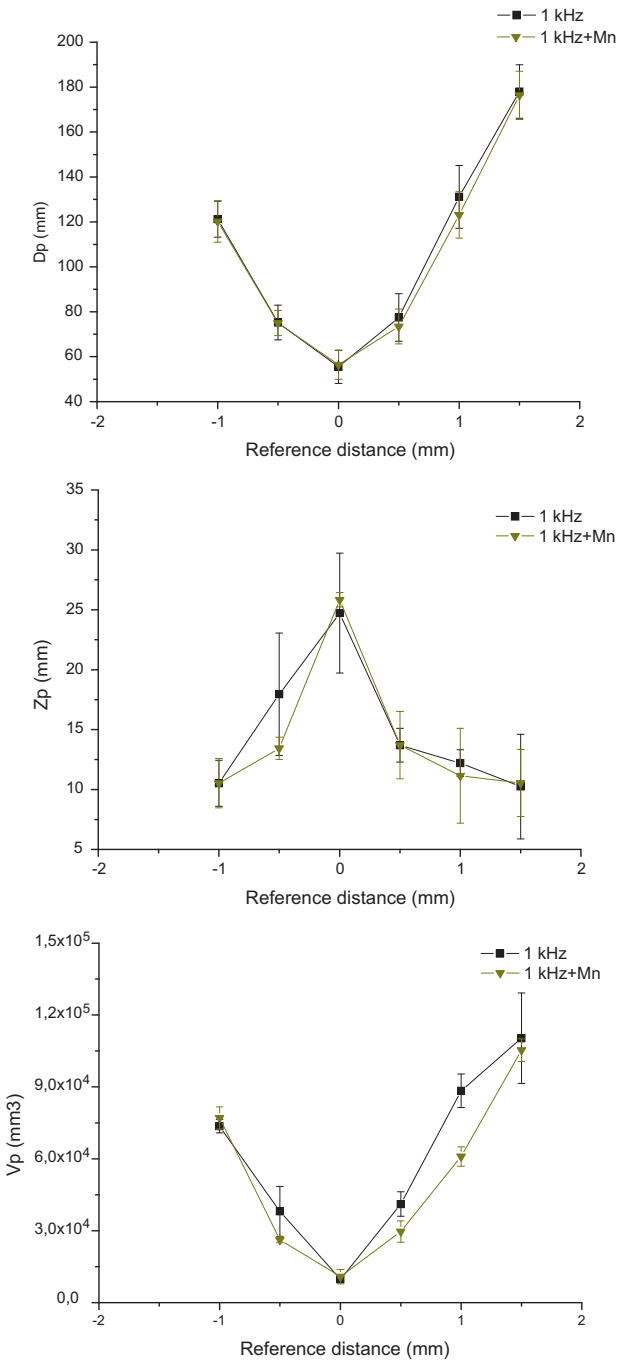

Fig. 5. Geometric parameters in function of reference distance for 1 kHz with and without Mn_2O_3 and 50 laser pulses.

3.2. Microstructure and composition

In order to analyze the effects appeared in the microstructure as a consequence of laser-matter interaction, a micro-structural analysis was carried out by means of scanning electron microscope, SEM.

In the first place, the composite obtained after the laser floating process was analyzed. Fig. 9 depicts the frontal view of the directional solidified sample. The micrograph shows how the microstructure was made up of faceted colonies with a size of around 100 μm that consisted of ordered zirconia fibers, light phase, within an alumina matrix, dark phase. Both phases were homogeneously distributed in the sample. The composition of the sample was determined by EDX analysis concluding that the sample was in the eutectic composition, Table 3.

After analysing the microstructure of the sample the effect produced by the laser machining was studied. As Fig. 10 shows, the eutectic microstructure remained invariant as in the processed areas as in the adjacent zones. Furthermore, as the results mentioned before showed, the machined diameter remained almost constant with the pulse number. Worth of mention is

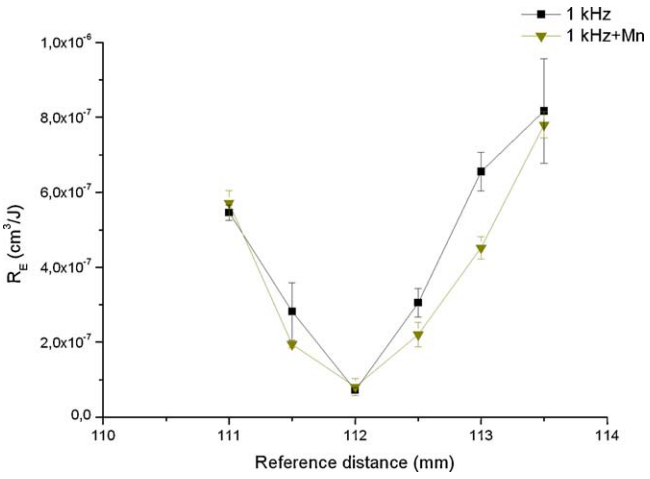

Fig. 6. Ablation yield in function of reference distance for 1 kHz with and without Mn_2O_3 and 50 laser pulses.

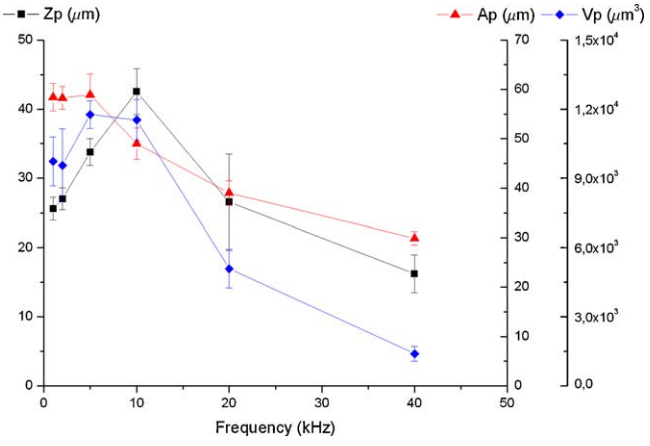

Fig. 7. Geometric parameters in function of working frequency for 50 laser pulses.

the fact that a cone was produced in the central zone, the depth of which increased with the pulse number. The micrographs of Fig. 11 depict how the microstructure was kept eutectic inside. No significant variations were observed in the morphology of

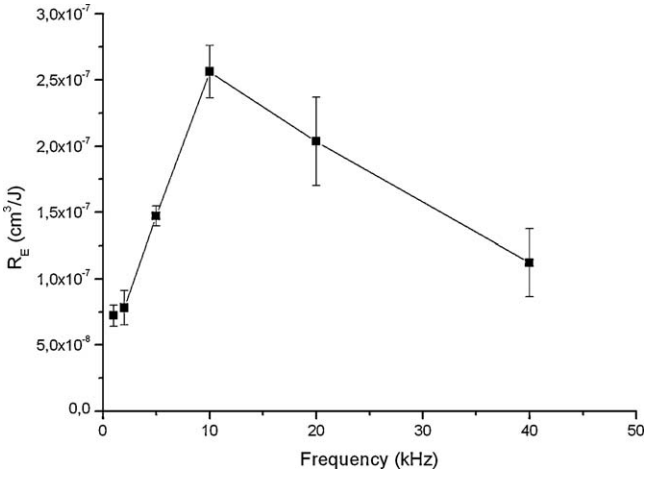

Fig. 8. Ablation yield in function of working frequency for 50 laser pulses.

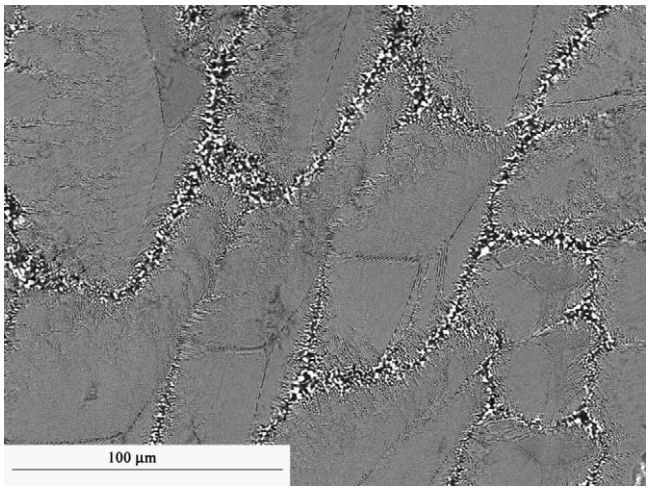

Fig. 9. Cross-sectional view of Al_2O_3–ZrO_2 (3%Y_2O_3) eutectic composite directionally solidified obtained by the laser floating zone technique.

Table 3
Composition of the Al_2O_3–ZrO_2 (3%Y_2O_3) eutectic composite.

Element	% weight	% atomic
O	39.96	64.82
Al	26.68	25.66
Y	3.99	1.16
Zr	29.37	8.36
Total	100.00	100.00

the holes caused by the addition of Mn_2O_3 to the eutectic composite. Likewise, the border of the hole presented a non-visible ordered phase the width of which increased with the pulse series or the working frequency, Fig. 12. Since the ablation process was of photothermal character, a heat affected zone, HAZ, was produced in the surroundings of the processed areas. The short interaction time between the laser and the substrate (a few nanoseconds) and the ceramic nature of the sample led to a bad thermal conduction of the heat produced during the process and a fast cooling that generated the formation of this phase. For the 50 pulses case, the size of the phase was around 4 μm whilst for 150 pulses could reach 6 μm. The elemental composition of this phase was characterized by EDX, concluding that the composition was the same of the former, Table 4.

Table 4
Composition of the phase produced in the border of the hole.

Element	% weight	% atomic
O	38.57	64.08
Al	25.92	25.54
Y	3.57	1.07
Zr	31.93	9.31
Total	100.00	100.00

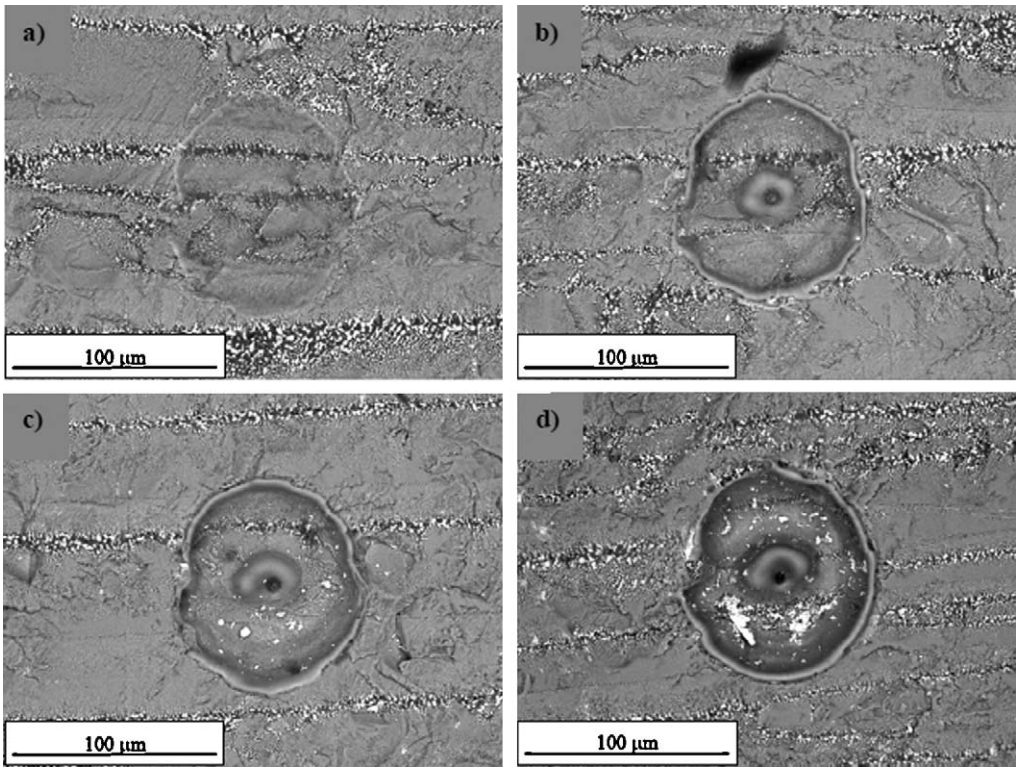

Fig. 10. Effect of laser machining in Al_2O_3–ZrO_2 (3%Y_2O_3) eutectic composite for 1 kHz and (a) 10 pulses, (b) 50 pulses, (c) 100 pulses and (d) 150 pulses.

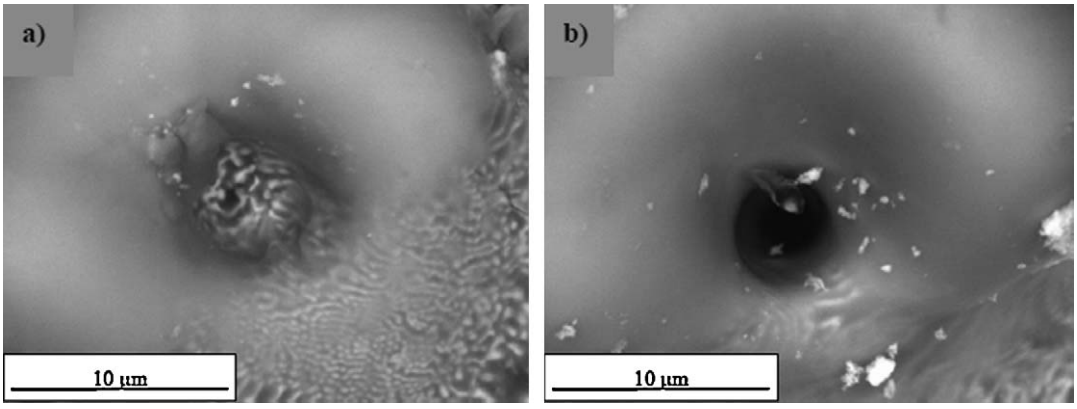

Fig. 11. Detail of the central cone obtained in Al_2O_3–ZrO_2 (3%Y_2O_3) eutectic composite for 1 kHz and (a) 50 pulses and (b) 150 pulses.

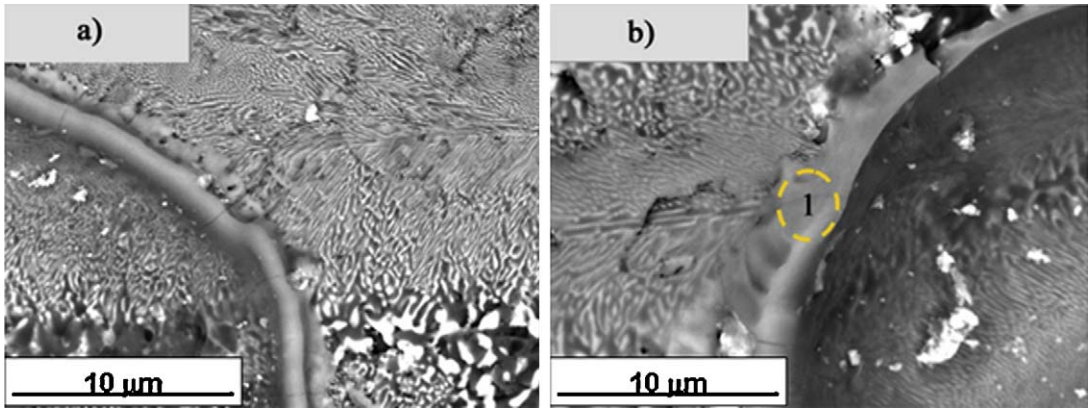

Fig. 12. Adjacent areas to the processed sample in the Al_2O_3–ZrO_2 (3%Y_2O_3) eutectic composite for 1 kHz and (a) 50 pulses and (b) 150 pulses.

4. Conclusions

The interaction phenomenon between NIR pulsed laser in the nanosecond range and the Al_2O_3–ZrO_2 (3%Y_2O_3) eutectic composite, directionally solidified, has been investigated and the geometric dimensions and ablation yields have been determined.

Different machining conditions have been explored modifying the laser power, the working frequency and the pulse number. Furthermore, the reference distance effect with respect to the focal plane has also been studied.

In all the cases, the addition of Mn_2O_3 only produces significant variations either in the geometric dimensions or in the ablation yield for low pulse number.

Laser interaction process depends on factors such as the substrate temperature, the plasma shield, the pulse number, the sample position with respect to the focal plane and the working frequency. The optimal conditions are not unique but they depend on if the target is to obtain a high ablation yield, to minimize the radiation affected zones, to obtain minimum diameter or maximum ablated depth.

Laser machining does not produce any significant variation in the microstructure and the composition of the processed areas is the same of the former.

Acknowledgements

Daniel Sola thanks the JAE-DOC program and the Science and Technology Inter-Ministry commission of Spain and FEDER founds of the EC under project MAT2009-13979-C03-03 for the financial support of his contract.

References

1. Steen W. *Laser material processing*. 3rd ed. Springer Verlag; 2003.
2. Bäuerle D. *Laser processing and chemistry*. 3rd ed. Springer; 2000.
3. Allmen M, Blatter A. *Laser-beam interactions with materials*. 2nd ed. Springer; 1995.
4. Pauleau Y. *Materials surface processing by directed energy techniques*. Elsevier; 2006.
5. Misawa H, Juodkazis S. *3D laser microfabrication*. Wiley; 2006.
6. Gamaly EG, Rode AV, Luther-Davies B. *J Appl Phys* 1999;**85**:4213–21.
7. Rode AV, Luther-Davies B, Gamaly EG. *J Appl Phys* 1999;**85**:4222–30.
8. Bulgakova NM, Bulgakov AV. *Appl Phys A* 2001;**73**:199–208.
9. Anisimov MA. *Sov Phys Usp* 1975;**17**:249–94.
10. Chichkov BN, Momma C, Nolte S, Von Alvensleben F, Tünnermann A. *Appl Phys A* 1996;**63**:109–15.
11. Momma C, Chichkov BN, Nolte S, Alvensleben F, Tünnermann A, Welling H, Wellegehausen B. *Opt Commun* 1996;**129**:134–42.
12. Bulgakov AV, Bulgakova NM. *Quant Electron* 1999;**29**:433–7.
13. Gusarov A, Smurov I. *J Appl Phys* 2005;**97**:014307.
14. Singh RK, Narayan J. *Phys Rev B* 1990;**41**:8843–59.
15. Amoruso S, Bruzzese R, Spinelli N, Velotta R. *J Phys B: At Mol Opt Phys* 1999;**32**:R131–72.
16. Willmott PR, Huber JR. *Rev Mod Phys* 2000;**72**:315–28.
17. Tode M, Takigawa Y, Masato M. *Met Mater Trans A* 2008;**39A**:130–4.
18. Braun A, Zimmer K, Bigl F. *Appl Surf Sci* 2000;**168**:178–81.
19. Kim JH, Lee S, Im HS. *Appl Phys A* 1999;**69**:S629–32.
20. Llorca J, Orera VM. *Prog Mater Sci* 2006;**51**:711–809.
21. Pastor JY, Poza P, Llorca J, Peña JI, Merino RI, Orera VM. *Mater Sci Eng A* 2001;**308**:241–9.
22. Laguna-Bercero MA, Larrea A, Merino RI, Peña JI, Orera VM. *J Ceram Soc* 2005;**88**:3215–7.
23. Ashbrook RL. *J Am Ceram Soc* 1977;**60**:428–35.
24. Orera VM, Merino RI, Pardo JA, Larrea A, Peña JI, González C, Poza P, Pastor JY, Llorca J. *Acta Mater* 2000;**48**:4683–9.
25. Schreck S, Zum Gahr KH. *Appl Surf Sci* 2005;**247**:616–22.
26. Miyoshi K, Farmer SC, Sayir A. *Tribol Int* 2005;**38**:974–86.
27. Sola D, Escartin A, Cases R, Peña JI. *Appl Surf Sci* 2011;**257**:5413–9.
28. Sola D, Ester FJ, Oliete PB, Peña JI. *J Eur Ceram Soc* 2011;**31**:1211–8.
29. Ester FJ, Sola D, Peña JI. *Bol Soc Esp Ceram* 2008;**6**:352–7.
30. Ester FJ, Peña JI. *Bol Soc Esp Ceram* 2007;**46**:240–6.
31. Samant AN, Dahotre NB. *J Eur Ceram Soc* 2009;**20**:969–93.
32. Samant AN, Du B, Dahotre NB. *Phys Stat Sol* 2009;**206**:1433–9.
33. Barin I. *Thermodynamical data of pure substances*, vols. 1 (Ag–Kr) and 2 (La–Zr), 3rd ed. VCH; 1995.
34. Lide DR. *Hand book of chemistry and physics*. 84th ed. CRC Press; 2003–2004.